Sp1-Induced Upregulation of LBX2-AS1 Aggravates The Progression of Glioblastoma By Targeting The miR-491-5p/LIF Axis

Wentao Li
Jiangsu Province Hospital and Nanjing Medical University First Affiliated Hospital
Ismatullah Soufiany
Jiangsu Province Hospital and Nanjing Medical University First Affiliated Hospital
Xiao Lyu
Jiangsu Province Hospital and Nanjing Medical University First Affiliated Hospital
Lin Zhao
Jiangsu Province Hospital and Nanjing Medical University First Affiliated Hospital
Chenfei Lu
Jiangsu Province Hospital and Nanjing Medical University First Affiliated Hospital
Yutian Wei
Jiangsu Province Hospital and Nanjing Medical University First Affiliated Hospital
Zhumei Shi
Jiangsu Province Hospital and Nanjing Medical University First Affiliated Hospital
Yongping You (yypl9@njmu.edu.cn)
Jiangsu Province Hospital and Nanjing Medical University First Affiliated Hospital

Research

Keywords: LBX2-AS1, miR-491-5p, LIF, EMT, angiogenesis, glioblastoma

Posted Date: March 1st, 2021

DOI: https://doi.org/10.21203/rs.3.rs-242079/v1

Abstract

Background: Mounting evidences have shown the importance of lncRNAs in tumorigenesis and cancer progression. LBX2-AS1 is an oncogenic lncRNA that has been found abnormally expressed in gastric cancer and lung cancer samples. Nevertheless, the biological function of LBX2-AS1 in glioblastoma (GBM) and potential molecular mechanism are largely unclear.

Methods: Relative levels of LBX2-AS1 in GBM samples and cell lines were detected by qRT-PCR and FISH. *In vivo* and *in vitro* regulatory effects of LBX2-AS1 on cell proliferation, epithelial-to-mesenchymal transition (EMT) and angiogenesis in GBM were examined through xenograft models and functional experiments, respectively. The interaction between Sp1 and LBX2-AS1 was assessed by ChIP. Through bioinformatic analyses, dual-luciferase reporter assay, RIP and Western blot, the regulation of LBX2-AS1 and miR-491-5p on the target gene leukemia Inhibitory factor (LIF) was identified.

Results: LBX2-AS1 was upregulated in GBM samples and cell lines, and its transcription was promoted by binding to the transcription factor Sp1. As a lncRNA mainly distributed in the cytoplasm, LBX2-AS1 upregulated LIF, and activated the LIF/STAT3 signaling by exerting the miRNA sponge effect on miR-491-5p, thus promoting cell proliferation, EMT and angiogenesis in GBM. Besides, LBX2-AS1 was unfavorable to the progression of glioma and the survival.

Conclusion: Upregulated by Sp1, LBX2-AS1 promotes the progression of GBM by targeting the miR-491-5p/LIF axis. It is suggested that LBX2-AS1 may be a novel diagnostic biomarker and therapeutic target of GBM.

Background

Glioblastoma multiforme (GBM, WHO IV) is the most lethal type of glioma (~50%), which mainly affects people older than 50 years and featured by local invasion and neovascularization [1-3]. Although therapeutic progression has been made on GBM, including surgery, radiotherapy, chemotherapy, and targeted therapy, its overall prognosis is extremely poor with the 5-year survival of lower than 10% [4-6]. It is well known that the generation and progression of glioma is complicated, involving gene mutations, epithelial-mesenchymal transition (EMT), excessive angiogenesis and other biological processes [7, 8]. So, a clear understanding of the molecular mechanism of GBM is conductive to advance therapeutic strategy and thus prolongs the survival.

LncRNAs (long non-coding RNAs) are over 200 nucleotides long, which are functional in epigenetic regulation, histone modification, transcription control and RNA metabolism [9, 10]. Current evidences have proven the regulatory effects of lncRNAs on cancer progression [11, 12]. L Salmena et al. [13] first proposed ceRNA theory, in which lncRNAs exert a sponge effect on miRNAs, therefore upregulating mRNAs that are targeted to the certain miRNAs. Recently, the lncRNA-miRNA-mRNA axis has been widely explored in multiple types of cancers. Z Sun et al. [14] suggested that MALAT1 promotes EMT and angiogenesis in colorectal carcinoma by sponging miR-126-5p. H Wang et al. [15] proved that the XIST-

miR-186-5p axis stimulates the proliferative and invasive potentials of NSCLC. J Zheng et al. [16] identified the role of CRNDE in aggravating glioma by regulating miR-384.

Recent studies have found that LBX2-AS1 is an oncogenic lncRNA that is highly expressed in gastric cancer, ovarian cancer and NSCLC [17-19]. Besides, LBX2-AS1 is also upregulated in glioma samples, and correlated to the prognosis [20, 21]. This study first detected the differential level of LBX2-AS1 in GBM tissues, and its oncogenic role and the underlying mechanism were further explored.

Materials And Methods

Collection of GBM samples

Thirty GBM samples were collected during surgery, including 20 primary GBM cases and 10 recurrent cases, and they were pathologically confirmed. In addition, 5 normal brain samples were collected during decompression surgery of traumatic brain injury at Neurosurgery Department, the First Affiliated Hospital of Nanjing Medical University, Nanjing, China. This study was reviewed and approved by the Clinical Research Ethic Committee of the First Affiliated Hospital of Nanjing Medical University.

Bioinformatic analyses

RNA-seq data were downloaded from The Cancer Genome Atlas (TCGA, http://cancergenome), Chinese Glioma Genome Atlas (CGGA, www.cgga.org) and Gene Expression Omnibus (GEO, https://www.ncbi.nlm.nih.gov/geo) for bioinformatic analyses. GO and KEGG were performed using DAVID (https://david.ncifcrf.gov/). The limma R package and clusterprofiler package were used for differential analysis and GSEA analysis, respectively.

Cell culture

Human glioma cell lines (U87, LN229, A172, T98G, U251), normal human astrocytes (NHA) and human umbilical vein endothelial cells (HUVECs) were provided by the American Type Culture Collection (ATCC). Primary GBM cell line (N3) was gifted from Beijing Tiantan Hospital. HEK293T cell line was provided by Cell Bank of the Chinese Academy of Sciences. Except for HUVECs cultured in EGM-2 (Lonza), the remaining were cultivated in DMEM containing 10% FBS. Cells were incubated at 37℃ in a humidified environment containing 5% CO_2.

qRT-PCR

Cells were lysed in TRIzol (Invitrogen, CA, USA) and the isolated RNA was reversely transcribed to cDNA using the PrimeScript RT (Takara, Nanjing, China). PARIS^{TM} Nuclear/Cytosol Fractionation Kit was used for isolating nuclear and cytoplasmic components. After preparing a PCR system using the SYBR Green Premix Ex Taq (Takara, Nanjing, China), PCR was conducted with U6 or GAPDH as the internal reference. Relative level was calculated using $2^{-\Delta\Delta Ct}$ method. Primer sequences are shown in Additional file 2: Table s4.

Fluorescence in situ hybridization (FISH)

RNA-FISH was conducted as previously described [22]. LBX2-AS1 probe was provided by RiboBio (Guangzhou, China). FISH-RNA signal in GBM cells and specimens were captured using a confocal microscope system (Zeiss LSM 700).

Cell transfection

Transfection of siRNAs, miRNA mimics and plasmids (Genechem, Shanghai, China) was conducted using Lipofectamine 2000 (Invitrogen). cDNAs that were complementary paired to LBX2-AS1, Sp1 and LIF were synthesized, which were cloned into pcDNA3.1 (Invitrogen). LBX2-AS1 shRNAs and negative control (sh-Ctrl) were synthesized by Genechem (Shanghai, China). Screening by puromycin at 48 h, stably expressed N3 and U87 cell lines were established. Small interfering RNA (siRNA) and short hairpin RNA (shRNA) sequences designed for specific targets are listed in Additional file 1: Table s1-3.

Western blot

Western blot was conducted as previously described [23]. The following primary antibodies were used: anti-LIF (Abcam, ab138002), anti-p-STAT3(Abcam, ab76315), anti-STAT3(Cell Signaling Technology, 12640), anti-Sp1(Cell Signaling Technology, 9389), anti-N-cadherin (Cell Signaling Technology, 13116), anti-E-cadherin (Cell Signaling Technology, 3195), anti-Vimentin (Cell Signaling Technology, 5741), anti-Snail (Cell Signaling Technology, 3879), anti-Slug (Cell Signaling Technology, 9585), anti-MMP9 (Abcam, ab76003), anti-VEGF (Abcam, ab69479), and anti-GAPDH (Cell Signaling Technology, 5174).

Cell proliferation assay

Proliferative potential of GBM cells was assessed by CCK-8, colony formation and EdU assay. In the first experiment, cells were seeded in a 96-well plate and absorbance at 450 nm was measured using Cell Counting Kit-8 (Dojindo, Shanghai, China). In colony formation assay, cells were seeded in a 6-well plate and cultivated for 14 days. Colonies were washed in PBS twice, fixed in 4% paraformaldehyde for 10 min and stained in 0.1% crystal violet for 30 min, which were captured under a microscope. EdU Apollo DNA *in vitro* kit (RiboBio, Guangzhou, China) was used for measuring DNA synthesis during the proliferative process of GBM cells. Cells seeded in a 6-well plate were incubated with 50 μM EdU for 2 h, followed by 30-min fixation in 4% paraformaldehyde and staining with Apollo and Hoechst 33342. EdU-positive cells were captured using a fluorescence microscope for counting.

Transwell assay

Transwell inserts (Corning, New York, USA) were pre-coated with 20 μg/μl Matrigel (BD Biosciences, New jersey, USA). 2×10^4 cells suspended in serum-free medium and culture medium containing 10% FBS were respectively applied at the top and bottom of the prepared insert. After 24-h cell culture, cells invaded from the top to the bottom were fixed in 4% paraformaldehyde for 10 min and dyed in 0.1% crystal violet for 30 min. Invasive cells in 3 random fields per sample were captured for counting.

3D tumor spheroid invasion assay

3D tumor spheroid invasion assay was conducted as previously described [24]. 2×10^5 cells in a 96-well plate were cultivated in complete medium containing spheroid formation matrix for 96 h, followed by adding Matrigel for embedding spheroids. Spheroids were captured at 0, 24, 48 and 72 h, respectively under a microscope, and the invasive area was evaluated using spheroids at 0 h as the reference.

Tube formation assay

1×10^4 HUVECs cultivated in conditioned medium of GBM cells were collected and seeded on a μ-Slide Angiogenesis coated with 10 μl Matrigel (BD Bioscience, New Jersey, NJ, USA) at 37°C for 30 min. After 3-h cell culture, tube formation was captured under an optical microscope.

Dual-luciferase reporter assay

Promoter-containing vector for LBX2-AS1, Sp1, TEAD2 and KLF5 (Genechem, Shanghai, China) were co-transfected into HEK293T cells, respectively. P1-wt (wild-type) and P1-mut (mutant) sequences were synthesized and cloned into pGL3-basic luciferase vectors (Promega, Madison, USA), which were co-transfected into HEK293T cells with Sp1 plasmid. In addition, luciferase vectors containing mutant or wild-type sequences in which miR-491-5p bound to promoter region of LBX2-AS1 or LIF were co-transfected into N3 or U87 cells with miR-491-5p mimic or negative control. Relative luciferase activity was measured using the Promega Dual-luciferase Reporter System, and normalized to that of Renilla luciferase activity.

Chromatin immunoprecipitation (ChIP)

EZ-ChIP Kit (Millipore, Billerica, MA, USA) was used for ChIP assay. Briefly, cells were cross-linked in 1% formaldehyde for 10 min and terminated by glycine. Cells were lysed to chromatin fragments by sonication. DNA/protein complex was incubated with 3 μg anti-Sp1 (Cell Signaling Technology, 9389). Anti-IgG (Millipore, 12–371) was used as the negative control. The special primers for P1 site, P2 site and P3 site are listed in Additional file 2: Table s5.

RNA immunoprecipitation (RIP)

Magna RIPTM RNA-Binding Protein Immunoprecipitation Kit (Millipore, Billerica, MA, USA) was used for RIP assay. Briefly, cell lysate was incubated with anti-Ago2(Abcam, ab32381), and anti-IgG (negatively control). A protein-RNA complex was captured, followed by removal of the protein. The magnetic beads were repeatedly washed with RIP washing buffer, and the immunoprecipitated RNA was quantified by performing qRT-PCR.

Immunohistochemistry (IHC)

After sacrifice, GBM tissues collected from nude mice were fixed in 4% paraformaldehyde, and paraffin embedded for preparation of tissue sections. Sections were incubated with anti-Ki-67, anti-LIF and anti-p-STAT3 for IHC.

Orthotopic GBM xenograft model

6-week-old male BALB/c nude mice were provided by Animal Core Facility of Nanjing Medical University. Twelve mice were used in the subcutaneous xenograft GBM model, with 6 mice in each group. They were respectively subcutaneously administrated with 1×10^7 U87 cells transfected with sh-NC or sh-LBX2-AS1#1. The growth of tumor was measured once a week and the volume was calculated: Tumor volume (mm^3) = 0.5 × the longest diameter (mm) × the shortest diameter^2 (mm^2). In the intracranial xenograft GBM model, 12 mice were randomly assigned to two groups, with 6 in each. They were respectively intracranially administrated with 2.5×10^5 U87 cells transfected with sh-NC or sh-LBX2-AS1#1 using a stereotaxis instrument. Tumors in mice was examined using optical imaging (IVIS spectrum, PerkinElmer, USA).

Statistical analysis

Statistical analyses were conducted using GraphPad software version 8.0 (GraphPad software, San Diego, CA, USA) or SPSS Statistics 23.0 (SPSS, Chicago, IL, USA). Differences between groups were compared by Student's *t* test or one-way ANOVA. Pearson's correlation test was performed for evaluating the correlation between two indexes. Kaplan-Meier survival analysis was performed, and the difference was compared by log-rank test. All experiments were repeated in triplicate, and data were expressed as mean ± standard error of the mean (SEM). A significant difference was considered at $p<0.05$ (*$p<0.05$, **$p<0.01$, ***$p<0.001$).

Results

Upregulation of LBX2-AS1 in glioblastoma

To identify differentially expressed lncRNAs between glioblastoma and normal samples, we analyzed RNA-seq data from TCGA, CGGA and GEO (GSE151352) using the limma R package (FDR < 0.05, $|Log_2FC| >1$). Upregulated and downregulated lncRNAs in GBM samples were illustrated in heatmap and volcano plots (**Fig.1a, Fig.s1a**). By selecting the intersection, LBX2-AS1, CRNDE, H19 and MIR210HG were predicted upregulated in all the three databases (**Fig.1b**). We subsequently analyzed their expression levels in 693 glioma samples from CGGA. Only LBX2-AS1 was significantly different between primary and recurrent cases both in low-grade glioma (LGG) and GBM (**Fig.1c**). In particular, LBX2-AS1 level was higher in GBM samples than that of low-grade glioma (**Fig.1d**). By assessing clinical features of glioma samples in TCGA and CGGA, it is indicated that LBX2-AS1 was highly expressed in mesenchymal (MES) glioma samples (**Fig.1e-f, Fig.s1b-c, Table s6-7**). It is generally considered that the transition from proneural (PN) to MES subtype is a hallmark for the malignant development and recurrence of glioma [25-27]. In addition, Kaplan-Meier survival analysis obtained the conclusion that LBX2-AS1 was

unfavorable to the overall survival of LGG and GBM (**Fig.1g**). Collectively, LBX2-AS1 was upregulated in GBM samples, and of significance in the malignant progression of glioma.

Bioinformatic analyses on LBX2-AS1 in GBM

Relative levels of LBX2-AS1 in normal human astrocytes (NHA), glioma cell lines (U251, U87, A172, T98G and LN229) and primary GBM cell line (N3) were measured by qRT-PCR (**Fig.2a**). N3 and U87 cells highly expressing LBX2-AS1 and U251 cells lowly expressing LBX2-AS1 were used in the following experiments. We synthesized three LBX2-AS1 shRNAs and tested their transfection efficacy in N3 and U87 cells, and finally, sh-LBX2-AS1#1 was selected for its excellent performance (**Fig.2b**). Moreover, transfection of pcDNA-LBX2-AS1 markedly upregulated LBX2-AS1 in N3, U87 and U251 cells (**Fig.2c**). Similarly, LBX2-AS1 level was higher in GBM samples collected in our center than that of normal brain samples, and notably, it was remarkably higher in recurrent GBM samples compared with that of primary ones (**Fig.2d**). RNA-FISH for quantification of LBX2-AS1 in GBM samples, as expected, was consistent with PCR results (**Fig.2e**). To assess the regulatory effect of LBX2-AS1 on malignant development of GBM, GBM samples from TCGA and CGGA were assigned to low group and high group, followed by determination of differentially expressed mRNAs and they were depicted in heatmap and volcano plots (**Fig.2f-g**). Since LBX2-AS1 was an oncogenic lncRNA, upregulated mRNAs in GBM samples were more concerned. According to the results yielded from gene set enrichment analysis (GSEA), high-level LBX2-AS1 was identified correlated to EMT, angiogenesis and extracellular matrix disassembly in GBM samples (**Fig.2h**). In addition, the Verhaak subtype signatures identified that the upregulation of LBX2-AS1 was positively correlated to MES subtype, but negatively correlated to PN subtype of glioma (**Fig.s1d**).

Knockdown of LBX2-AS1 suppresses proliferative potential, angiogenesis and EMT of GBM

Colony formation assay revealed that knockdown of LBX2-AS1 in N3 and U87 cells markedly reduced colony numbers, indicating the suppressed proliferative potential (**Fig.3a**). Cell viability of GBM was consistently reduced by transfection of sh-LBX2-AS1 (**Fig.3b**). 3D tumor spheroid invasion assay obtained the conclusion that knockdown of LBX2-AS1 inhibited invasive ability of GBM cell spheroids (**Fig.3c**), which was further validated in transwell assay (**Fig.3d**). Compared with negative control, the tube formation ability of HUVECs cultivated in conditioned medium of N3 and U87 cells transfected with either sh-LBX2-AS1#1 or sh-LBX2-AS1#2 was attenuated (**Fig.3e**). To assess the *in vivo* regulatory effects of LBX2-AS1 on tumorigenesis of GBM cells, we established xenograft model in nude mice administrated with U87 cells intervened by LBX2-AS1. Compared with control group, knockdown of LBX2-AS1 obviously slowed down the growth rate of tumor in nude mice (**Fig.3f-g**). We further detected EMT markers in GBM cells regulated by LBX2-AS1. Protein levels of N-cadherin, Vimentin were downregulated, while E-cadherin was upregulated in N3 and U87 cells with LBX2-AS1 knockdown (**Fig.3h**). Overexpression of LBX2-AS1 obtained opposite expression changes of them (**Fig.3i**). Taken together, knockdown of LBX2-AS1 suppressed cell proliferation, angiogenesis and EMT in GBM cells.

Sp1 upregulates LBX2-AS1 in GBM samples

We next explored why LBX2-AS1 was abnormally upregulated in GBM samples. The top 10 scored transcription factors that could bind to the promoter region of LBX2-AS1 were screened out using JASPAR (http://jaspar.genereg.net/) (**Fig.4a**). Relative levels of them in GBM samples, and their correlation to LBX2-AS1 were assessed by RNA- seq data from TCGA and CGGA (**Fig.4b, Fig.s2a**). Finally, three transcription factors intersected from the two databases, including Sp1, TEAD2 and KLF5 were selected for further investigations (**Fig.4c**). Promoter-containing vector for LBX2-AS1 and transcription factors were co-transfected into HEK293T cells with negative control, followed by measurement of relative luciferase activity, and that of Sp1 remained the highest (**Fig.4d**). A positive correlation was detected between relative levels of Sp1 and LBX2-AS1 in 30 clinical specimens of GBM, which was consistent with the correlation analysis in TCGA and CGGA (**Fig.4e, Fig.s2b**). Knockdown of Sp1 markedly downregulated LBX2-AS1, while overexpression of Sp1 upregulated it in N3 and U87 cells (**Fig.4f-g, Fig.s2c**). Through analyzing ChIP-seq data of transcription factors obtained from ENCODE database and putative transcription factors obtained from JASPAR in UCSC (http://genome.ucsc.edu/), Sp1 was found enriched in the promoter region of LBX2-AS1 (**Fig.4h**). The top three scored potential sites, where Sp1 bound to LBX2-AS1 were named as P1, P2 and P3 (**Fig.4i**). Later, ChIP assay confirmed that Sp1 was enriched in P1 site in HEK293T cells (**Fig.4j**). After mutating P1 site in the promoter region of LBX2-AS1, overexpression of Sp1 did not significantly affect relative luciferase activity, proving the direct interaction between Sp1 and LBX2-AS1 at P1 site (**Fig.4k-l**). Therefore, we have confirmed that Sp1 induced upregulation of LBX2-AS1 in GBM samples.

LBX2-AS1 exerts a sponge effect on miR-491-5p

A growing number of evidences have shown that lncRNAs abolish the regulatory effect of miRNAs on their target mRNAs, serving as ceRNAs [13, 28]. Subcellular distribution and RNA-FISH clarified that LBX2-AS1 was mainly distributed in the cytoplasm, suggesting the potential function of LBX2-AS1 as a ceRNA (**Fig.5a-b**). We identified 4 candidate miRNAs with complementary sites to LBX2-AS1 using starBase (http://starbase.sysu.edu.cn/) and LncBase (http://carolina.imis.athena-innovation.gr/diana_tools/web/index.php) (**Fig.5c**). Compared with control group, luciferase activity of pGLR-basic vector containing LBX2-AS1 was markedly reduced by overexpression of miR-491-5p in HEK293T cells (**Fig.5d**). Subsequently, RIP assay revealed that LBX2-AS1 and miR-491-5p could directly interact with Ago2 (**Fig.5e**), which is the core component of the RNA-induced silencing complex (RISC) involved in miRNAs-induced mRNA downregulation [29]. After mutation of the complementary sites of miR-491-5p to LBX2-AS1, relative luciferase activity of the vector was unable to be affected by miR-491-5p, confirming the specific interaction between LBX2-AS1 and miR-491-5p (**Fig.5f-g**). Regardless of LGG samples in TCGA or GBM specimens collected in our center, miR-491-5p was negatively correlated to LBX2-AS1 (**Fig.5h-i**). As expected, LBX2-AS1 negatively regulated miR-491-5p in N3 and U87 cells (**Fig.5j-k**). A series of functional experiments showed that the suppressed proliferative, invasive and angiogenic potentials of N3 and U87 cells with LBX2-AS1 knockdown were partially reversed by silence of miR-491-5p (**Fig.5l-n**). Collectively, LBX2-AS1 negatively regulated miR-491-5p by exerting the sponge effect on it.

LIF is the target mRNA of miR-491-5p and indirectly regulated by LBX2-AS1

The abovementioned data have confirmed the ceRNA function of LBX2-AS1, we thereafter identified the target mRNA of LBX2-AS1/miR-491-5p axis in the ceRNA network. Through GSEA, GO and KEGG analyses, we found that LBX2-AS1 participated in the regulation of the JAK-STAT3 signaling pathway (**Fig.6a, Fig.s3a**). A total of 3 candidate target mRNAs were finally obtained after a comprehensive analysis on putative targets of miR-491-5p in starbase, upregulated genes regulated by LBX2-AS1 in TCGA and CGGA, and JAK-STAT3 signaling-related genes, including SOCS3, CLCF1 and LIF (**Fig.6b**). qRT-PCR demonstrated that overexpression of miR-491-5p significantly downregulated LIF in N3 and U87 cells, and knockdown of miR-491-5p yielded the opposite result (**Fig.6c, Fig.s3b**). Meanwhile, relative level of LIF was positively correlated to LBX2-AS1, but negatively correlated to miR-491-5p in 30 GBM specimens (**Fig.s3c-d**), which were consistent with correlation analyses using TCGA and CGGA databases (**Fig.s3e-f**). Dual-luciferase reporter assay revealed that transfection of miR-491-5p mimics reduced luciferase activity of LIF-WT vector, whilst it did not influence that of LIF-MUT vector, indicating the direct binding of miR-491-5p in LIF 3'-UTR (**Fig.6d-e**). RIP assay demonstrated that LIF was able to be enriched in anti-Ago2 (**Fig.6f**). Knockdown of LBX2-AS1 resulted in a significant increase in the recruitment of Ago2 in the LIF transcript, while overexpression of LBX2-AS1 increased the enrichment of LBX2-AS1 in anti-Ago2, but decreased that of LIF in anti-Ago2 (**Fig.6g-h**). It is suggested that LBX2-AS1 competed with LIF transcript for Ago2-induced RISC. Transfection of miR-491-5p inhibitor markedly upregulated protein level of LIF in N3 and U87 cells, and transfection of miR-491-5p mimics resulted in the opposite trend (**Fig.6i**). Besides, knockdown of LBX2-AS1 downregulated both protein and mRNA levels of LIF (**Fig.6j, Fig.s3g**). We further assessed the LBX2-AS1-miR-491-5p-LIF axis. Interestingly, knockdown of LBX2-AS1 decreased luciferase activity of LIF-WT in HEK293T cells, and the decline was reversed by silence of miR-491-5p. Overexpression of LBX2-AS1, conversely, increased luciferase activity of LIF-WT, which was abolished by overexpression of miR-491-5p (**Fig.6k-l**). Protein and mRNA levels of LIF regulated by LBX2-AS1 and miR-491-5p were similarly identified (**Fig.6m-n, Fig.s3h-i**). As a result, the LBX2-AS1-miR-491-5p-LIF axis involved in GBM has been confirmed.

LIF advances malignant phenotypes of GBM cells*via* the LIF-STAT3 axis

According to the Hallmark and GO gene sets yielded from GSEA, high-level LIF was identified correlated to EMT, angiogenesis and extracellular matrix disassembly in GBM samples, which was consistent with those of LBX2-AS1 (**Fig.s4a**). Transfection efficacy of si-LIF and pcDNA-LIF in N3 and U87 cells was examined by both qRT-PCR and Western blot (**Fig.s4b-c**). A series of *in vitro* experiments were carried out to assess the effect of LIF as the component in the ceRNA network on triggering malignant phenotypes of GBM. Data of CCK-8 and EdU assay both concluded that overexpression of LBX2-AS1 could abolish the inhibitory effect of si-LIF on proliferative potential of GBM cells (**Fig.7a-c**). Later, the suppressed invasive ability of N3 and U87 cells transfected with si-LIF was abolished by overexpression of LBX2-AS1 (**Fig.7d-f**). Knockdown of LIF markedly inhibited angiogenesis of GBM, but it was reversed by overexpression of LBX2-AS1 (**Fig.7g**). Serving as a cytokine of the IL-6 family, LIF activates the JAK/STAT3, MAPK and PI3K signaling pathways by binding to the specific receptor LIFR [30]. The activation of the LIF/STAT3 signaling results in nuclear translocation of phosphorylated STAT3, thus initialing the transcription of downstream genes that are responsible for mediating EMT, angiogenesis and other biological activities.

Here, knockdown of LBX2-AS1 downregulated p-STAT3, rather than the total STAT3 in N3 and U87 cells, and the downregulated p-STAT3 was rescued by overexpression of LIF (**Fig.7h**). On the contrary, overexpression of LBX2-AS1 activated the LIF/STAT3 signaling, but it was reversed by silence of LIF (**Fig.7i**). miR-491-5p was also capable of LBX2-AS1-regulated expression change of LIF (**Fig.s4d-e**). Taken together, LBX2-AS1 mediated proliferation, EMT and angiogenesis by the LIF/STAT3 signaling, thereafter promoting the development of GBM.

In vivo knockdown of LBX2-AS1 slows down the growth of glioma in nude mice.

To assess the *in vivo* function of LBX2-AS1 in GBM, 2.5×10^5 luciferase-labeled U87 cells transfected with sh-LBX2-AS1#1 or sh-ctrl were intracranially administrated in nude mice. The growth of tumor was evaluated using optical imaging. Compared with control group, the volume of xenograft tumor tissues collected from LBX2-AS1 knocking-down group was remarkably smaller, and the survival rate was much higher (**Fig.8a-b**). IHC results showed lower positive expressions of Ki-67, LIF and p-STAT3 in tumor sections from LBX2-AS1 knocking-down group than those of controls (**Fig.8c**).

Discussion

Cancer-associated functions of lncRNAs have been highlighted, and they are potential biomarkers or therapeutic targets [11, 31]. Currently, the potential function of lncRNAs in GBM has been widely investigated [32, 33]. Through bioinformatic analyses using online databases, we have found that LBX2-AS1 was upregulated in GBM samples, and positively correlated to tumor staging of glioma. A high level of LBX2-AS1 predicted poor prognosis of glioma. Notably, LBX2-AS1 level was much higher in recurrent GBM cases than that of primary ones, indicating a potential relationship between LBX2-AS1 and GBM recurrence. The following *in vitro* experiments have demonstrated that LBX2-AS1 promoted proliferative, invasive and angiogenic capacities of GBM, serving as an oncogenic lncRNA. We believed that LBX2-AS1 was a promising biomarker that could be applied to the diagnosis and treatment of GBM.

Some lncRNAs are dysregulated in human cancers, however, why they are dysregulated have not been fully elucidated. The transcription of lncRNAs is mediated by transcription factors and epigenic regulatory factors [34-36]. Using JASPAR and ENCODE, multiple Sp1 binding sites were identified in the promoter region of LBX2-AS1. Furthermore, Sp1 was confirmed to activate the transcription of LBX2-AS1 through ChIP and dual luciferase reporter assay.

Subcellular distribution determines the role of lncRNAs in regulating malignant phenotypes of cancer cells [37, 38]. LBX2-AS1 was both expressed in cell nuclei and cytoplasm, which was more pronounced in the latter. Cytoplasmic lncRNAs have been widely recognized for their ceRNA function. By competitively sponging miRNAs, lncRNAs prevent the Ago-dependent degradation of target mRNAs that bind to miRNAs [28, 39]. As RIP assay shown, LBX2-AS1 could interact with Ago2, suggesting that LBX2-AS1 was able to exert the sponge effect. Subsequently, miR-491-5p was proven to be a potential target of LBX2-AS1. It is reported that miR-491-5p can alleviate the malignant progression of glioma [40]. Our findings showed a

negative correlation between relative levels of LBX2-AS1 and miR-491-5p. Importantly, the suppressed proliferative, invasive and angiogenic potentials of GBM cells by knockdown of LBX2-AS1 could be reversed by silence of miR-491-5p. Hence, we have proven that LBX2-AS1 exerted its oncogenic role in GBM by sponging miR-491-5p as a ceRNA.

According to the prediction using starBase, LIF was identified as a potential target of miR-491-5p, which was further confirmed by experiments. LBX2-AS1 could positively regulate LIF level in GBM cells, while LIF level was negatively regulated by miR-491-5p. Previous evidences have shown the upregulation of LIF in solid tumor samples, which mediates the growth, invasiveness and metastasis of tumor cells [41]. Through activating the STAT3 signaling, LIF boosts the proliferative and invasive capacities of choriocarcinoma cells [42]. The self-renewal of glioma-initiating cells is achieved by the LIF/STAT3 signaling [43]. Shi et al. [44] revealed the biological significance of LIF in triggering the development and chemotherapy resistance of pancreatic ductal adenocarcinoma. This study first reported that LBX2-AS1 regulated the LIF/STAT3 signaling as a ceRNA in GBM. STAT3 is a transcription factor that is well recognized for mediating downstream gene transcription, such as those involved in the regulation of EMT and angiogenesis. Jin W et al. [45] proposed that STAT3 stimulates EMT in tumor cells by upregulating Snail and Slug. VEGF and MMP9 are key mediators of tumor angiogenesis, which are regulated by STAT3 [46, 47]. Our results showed that knockdown of LIF inhibited the activation of the LIF/STAT3 signaling, manifested as downregulated Snail, Slug, MMP9 and VEGF. Meanwhile, angiogenesis and EMT of GBM were suppressed as well, which could be reversed by overexpression of LBX2-AS1.

Two limitations in the present study should be considered. Firstly, we proved that Sp1 could bind to the promoter region of LBX2-AS1 and thus regulated its transcription. The specific mechanism, however, remains unclear. Secondly, LBX2-AS1 was highly expressed in recurrent GBM samples. The potential interaction between LBX2-AS1 and drug resistance of GBM needs further explorations.

Conclusions

LBX2-AS1 is upregulated in GBM and correlated to the poor prognosis. It exerts the sponge effect on miR-491-5p, thus upregulating LIF and activating the LIF/STAT3 signaling. The LIF/STAT3 signaling is responsible for promoting proliferation, EMT and angiogenesis of GBM. In addition, Sp1 is identified to induce the expression of LBX2-AS1, although the underlying mechanism needs further investigation. Our findings suggested that LBX2-AS1 may be a novel prognostic marker and therapeutic target of GBM.

Abbreviations

lncRNA: Long non-coding RNA; ceRNAs: Competing endogenous RNAs; GBM: Glioblastoma multiforme; EMT: epithelial-to-mesenchymal transition; HUVEC: Human umbilical vein endothelial cell; HEK293T: Human embryonic kidney 293 T; DMEM: Dulbecco's modified Eagle's medium; ANOVA: Analysis of variance; Ago2: Argonaute 2; LIF: leukemia Inhibitory factor; 3'-UTR: 3'-untranslated region.

Declarations

Acknowledgements
Not applicable.

Funding

This work was supported by National Nature Science Foundation of China (No. 81772679, 81974389, and 81872058); Natural Science Foundation of Jiangsu Province of China (BK20192008); Jiangsu Province's Key Discipline (ZDXKA2016001); The Priority Academic Program Development of Jiangsu Higher Education Institutions (PAPD); Science and Technology Development Fund of Nanjing Medical University (JX218317201711010); Key R&D Program (Social Development) Projects in Jiangsu Province (KY218ZX180013).

Availability of data and materials
The datasets used and analyzed during the current study are available from the corresponding author on reasonable request.

Authors' contributions
WTL mainly did the experiment and wrote the paper, IS and XL helped do the cell experiment and review the manuscript, CFL and YTW helped do analysis and interpretation of data. LZ and ZMS mainly constructed the idea of this article and provided administrative, technical and material support. All authors read and approved the final manuscript.

Ethics approval and consent to participate

The study was approved by the Ethics Committee of Nanjing Medical University and written informed consent was obtained from all patients.

Consent for publication
Not applicable.

Competing interests
All authors declare that they have no competing interests.

References

1. V A Cuddapah, S Robel, S Watkins, et al. A neurocentric perspective on glioma invasion. Nat Rev Neurosci. 2014;15(7):455-65.
2. T Demuth, M E Berens. Molecular mechanisms of glioma cell migration and invasion. J Neurooncol. 2004;70(2):217-28.
3. O Kargiotis, J S Rao, A P Kyritsis. Mechanisms of angiogenesis in gliomas. J Neurooncol. 2006;78(3):281-93.

4. T Jiang, D H Nam, Z Ram, et al. Clinical practice guidelines for the management of adult diffuse gliomas. Cancer Lett. 2021;499:60-72.
5. A M Molinaro, J W Taylor, J K Wiencke, et al. Genetic and molecular epidemiology of adult diffuse glioma. Nat Rev Neurol. 2019;15(7):405-17.
6. R Stupp, M E Hegi, W P Mason, et al. Effects of radiotherapy with concomitant and adjuvant temozolomide versus radiotherapy alone on survival in glioblastoma in a randomised phase III study: 5-year analysis of the EORTC-NCIC trial. Lancet Oncol. 2009;10(5):459-66.
7. J I Bastien, K A McNeill, H A Fine. Molecular characterizations of glioblastoma, targeted therapy, and clinical results to date. Cancer. 2015;121(4):502-16.
8. T T Lah, M Novak, B Breznik. Brain malignancies: Glioblastoma and brain metastases. Semin Cancer Biol. 2020;60:262-73.
9. J J Quinn, H Y Chang. Unique features of long non-coding RNA biogenesis and function. Nat Rev Genet. 2016;17(1):47-62.
10. R W Yao, Y Wang, L L Chen. Cellular functions of long noncoding RNAs. Nat Cell Biol. 2019;21(5):542-51.
11. M Huarte. The emerging role of lncRNAs in cancer. Nat Med. 2015;21(11):1253-61.
12. J R Prensner, A M Chinnaiyan. The emergence of lncRNAs in cancer biology. Cancer Discov. 2011;1(5):391-407.
13. L Salmena, L Poliseno, Y Tay, et al. A ceRNA hypothesis: the Rosetta Stone of a hidden RNA language? Cell. 2011;146(3):353-8.
14. Z Sun, C Ou, J Liu, et al. YAP1-induced MALAT1 promotes epithelial-mesenchymal transition and angiogenesis by sponging miR-126-5p in colorectal cancer. Oncogene. 2019;38(14):2627-44.
15. H Wang, Q Shen, X Zhang, et al. The Long Non-Coding RNA XIST Controls Non-Small Cell Lung Cancer Proliferation and Invasion by Modulating miR-186-5p. Cell Physiol Biochem. 2017;41(6):2221-29.
16. J Zheng, X Liu, P Wang, et al. CRNDE Promotes Malignant Progression of Glioma by Attenuating miR-384/PIWIL4/STAT3 Axis. Mol Ther. 2016;24(7):1199-215.
17. J Cao, H Wang, G Liu, et al. LBX2-AS1 promotes ovarian cancer progression by facilitating E2F2 gene expression via miR-455-5p and miR-491-5p sponging. J Cell Mol Med. 2020.
18. L X Tang, S F Su, Q Wan, et al. Novel long non-coding RNA LBX2-AS1 indicates poor prognosis and promotes cell proliferation and metastasis through Notch signaling in non-small cell lung cancer. Eur Rev Med Pharmacol Sci. 2019;23(17):7419-29.
19. Z Yang, X Dong, M Pu, et al. LBX2-AS1/miR-219a-2-3p/FUS/LBX2 positive feedback loop contributes to the proliferation of gastric cancer. Gastric Cancer. 2020;23(3):449-63.
20. R Liang, Y Zhi, G Zheng, et al. Analysis of long non-coding RNAs in glioblastoma for prognosis prediction using weighted gene co-expression network analysis, Cox regression, and L1-LASSO penalization. Onco Targets Ther. 2019;12:157-68.

21. S Subhash, N Kalmbach, F Wegner, et al. Transcriptome-wide Profiling of Cerebral Cavernous Malformations Patients Reveal Important Long noncoding RNA molecular signatures. Sci Rep. 2019;9(1):18203.
22. Y Cui, D Hu, L M Markillie, et al. Fluctuation localization imaging-based fluorescence in situ hybridization (fliFISH) for accurate detection and counting of RNA copies in single cells. Nucleic Acids Res. 2018;46(2):e7.
23. A L Zeng, W Yan, Y W Liu, et al. Tumour exosomes from cells harbouring PTPRZ1-MET fusion contribute to a malignant phenotype and temozolomide chemoresistance in glioblastoma. Oncogene. 2017;36(38):5369-81.
24. L Fan, Z Chen, X Wu, et al. Ubiquitin-Specific Protease 3 Promotes Glioblastoma Cell Invasion and Epithelial-Mesenchymal Transition via Stabilizing Snail. Mol Cancer Res. 2019;17(10):1975-84.
25. K P L Bhat, V Balasubramaniyan, B Vaillant, et al. Mesenchymal differentiation mediated by NF-kappaB promotes radiation resistance in glioblastoma. Cancer Cell. 2013;24(3):331-46.
26. M D Prados, S A Byron, N L Tran, et al. Toward precision medicine in glioblastoma: the promise and the challenges. Neuro Oncol. 2015;17(8):1051-63.
27. Y Wang, T Jiang. Understanding high grade glioma: molecular mechanism, therapy and comprehensive management. Cancer Lett. 2013;331(2):139-46.
28. D W Thomson, M E Dinger. Endogenous microRNA sponges: evidence and controversy. Nat Rev Genet. 2016;17(5):272-83.
29. G Hutvagner, M J Simard. Argonaute proteins: key players in RNA silencing. Nat Rev Mol Cell Biol. 2008;9(1):22-32.
30. N A Nicola, J J Babon. Leukemia inhibitory factor (LIF). Cytokine Growth Factor Rev. 2015;26(5):533-44.
31. M E Forrest, A M Khalil. Review: Regulation of the cancer epigenome by long non-coding RNAs. Cancer Lett. 2017;407:106-12.
32. Z Peng, C Liu, M Wu. New insights into long noncoding RNAs and their roles in glioma. Mol Cancer. 2018;17(1):61.
33. F Yang, X Liu, Y Liu, et al. miR-181d/MALT1 regulatory axis attenuates mesenchymal phenotype through NF-kappaB pathways in glioblastoma. Cancer Lett. 2017;396:1-9.
34. M Huarte, M Guttman, D Feldser, et al. A large intergenic noncoding RNA induced by p53 mediates global gene repression in the p53 response. Cell. 2010;142(3):409-19.
35. M Sun, X H Liu, K H Lu, et al. EZH2-mediated epigenetic suppression of long noncoding RNA SPRY4-IT1 promotes NSCLC cell proliferation and metastasis by affecting the epithelial-mesenchymal transition. Cell Death Dis. 2014;5:e1298.
36. Y Zhang, Y X Huang, D L Wang, et al. LncRNA DSCAM-AS1 interacts with YBX1 to promote cancer progression by forming a positive feedback loop that activates FOXA1 transcription network. Theranostics. 2020;10(23):10823-37.

37. G St Laurent, C Wahlestedt, P Kapranov. The Landscape of long noncoding RNA classification. Trends Genet. 2015;31(5):239-51.
38. K C Wang, H Y Chang. Molecular mechanisms of long noncoding RNAs. Mol Cell. 2011;43(6):904-14.
39. N T Schirle, J Sheu-Gruttadauria, I J MacRae. Structural basis for microRNA targeting. Science. 2014;346(6209):608-13.
40. X Li, Y Liu, K J Granberg, et al. Two mature products of MIR-491 coordinate to suppress key cancer hallmarks in glioblastoma. Oncogene. 2015;34(13):1619-28.
41. C Zhang, J Liu, J Wang, et al. The emerging role of leukemia inhibitory factor in cancer and therapy. Pharmacol Ther. 2020:107754.
42. J S Fitzgerald, S A Tsareva, T G Poehlmann, et al. Leukemia inhibitory factor triggers activation of signal transducer and activator of transcription 3, proliferation, invasiveness, and altered protease expression in choriocarcinoma cells. Int J Biochem Cell Biol. 2005;37(11):2284-96.
43. S Penuelas, J Anido, R M Prieto-Sanchez, et al. TGF-beta increases glioma-initiating cell self-renewal through the induction of LIF in human glioblastoma. Cancer Cell. 2009;15(4):315-27.
44. Y Shi, W Gao, N K Lytle, et al. Targeting LIF-mediated paracrine interaction for pancreatic cancer therapy and monitoring. Nature. 2019;569(7754):131-35.
45. W Jin. Role of JAK/STAT3 Signaling in the Regulation of Metastasis, the Transition of Cancer Stem Cells, and Chemoresistance of Cancer by Epithelial-Mesenchymal Transition. Cells. 2020;9(1).
46. D E Johnson, R A O'Keefe, J R Grandis. Targeting the IL-6/JAK/STAT3 signalling axis in cancer. Nat Rev Clin Oncol. 2018;15(4):234-48.
47. K Kessenbrock, V Plaks, Z Werb. Matrix metalloproteinases: regulators of the tumor microenvironment. Cell. 2010;141(1):52-67.

Figures

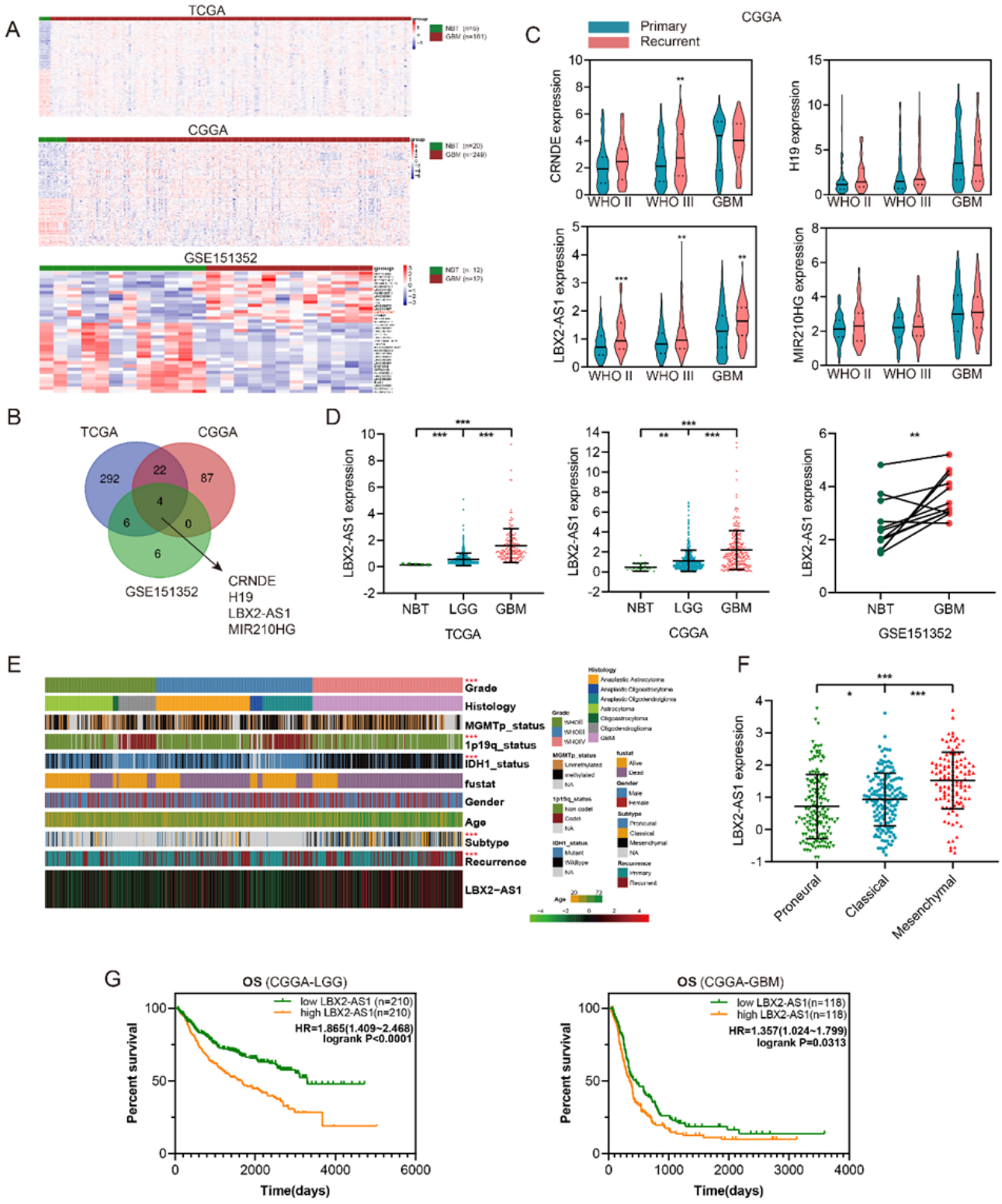

Figure 1

Upregulation of LBX2-AS1 in GBM samples. (A) Hierarchical cluster analysis of lncRNA expressions between normal samples and GBM samples in TCGA, CGGA and GEO (GSE151352) datasets. (B) Insertions of differentially expressed lncRNAs identified in TCGA, CGGA and GEO (GSE151352) datasets. (C) Relative levels of LBX2-AS1, CRNDE, H19 and MIR210HG in primary and recurrent glioma samples. (D) Relative levels of LBX2-AS1 in GBM samples from TCGA, CGGA and GEO (GSE151352) datasets. (E)

Heatmap of the associations between the expression level of LBX2-AS1 and clinicopathological features of glioma in CGGA dataset. (F) Relative levels of LBX2-AS1 in glioma samples from CGGA dataset categorized by transcription subtypes. (G) Kaplan-Meier survival analysis on low-grade glioma and glioblastoma patients based on LBX2-AS1 levels in CGGA dataset. *p<0.05, **p<0.01, ***p<0.001.

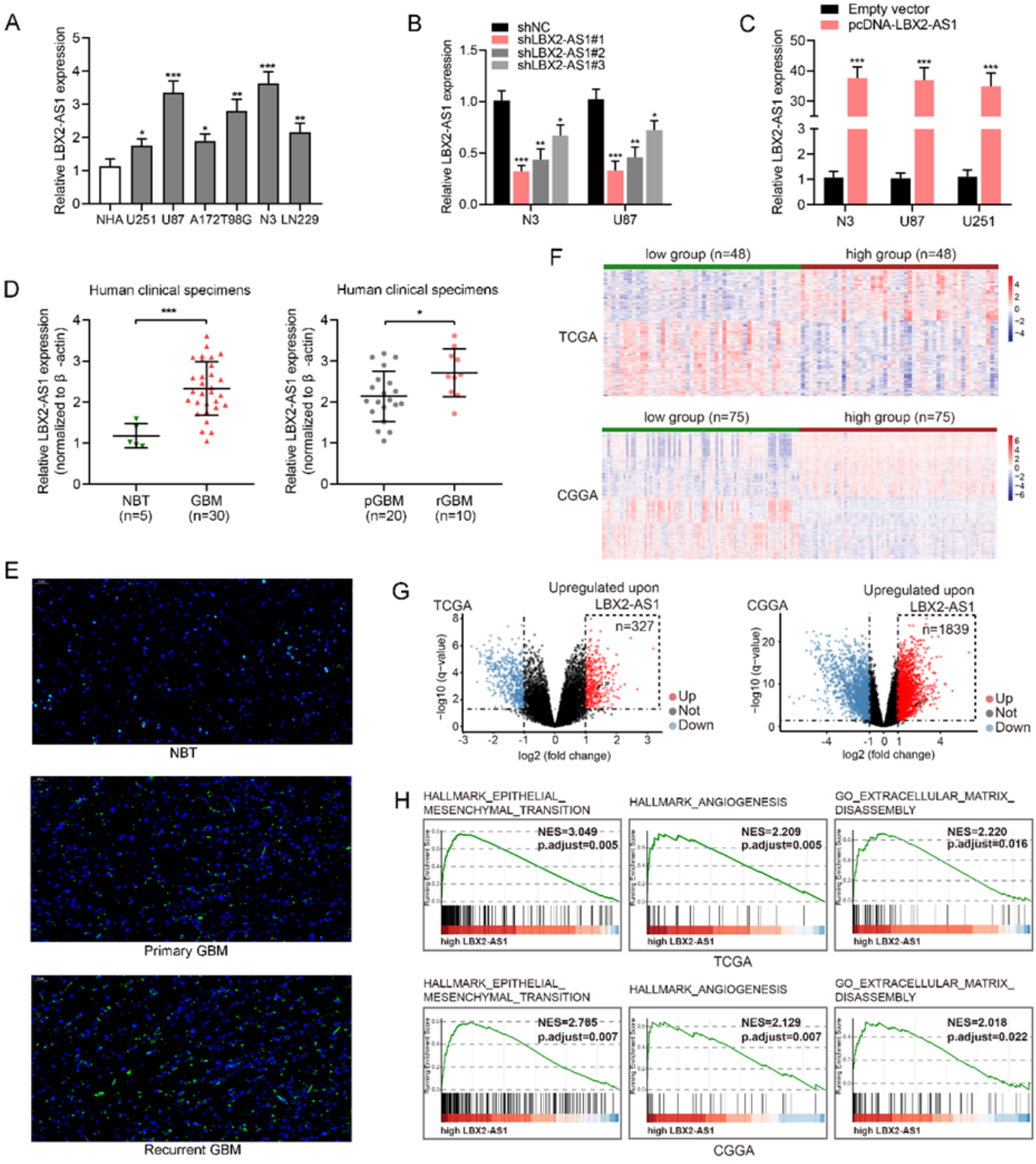

Figure 2

Bioinformatic analyses on LBX2-AS1 in GBM. (A) Relative levels of LBX2-AS1 in normal human astrocytes (NHA) and glioma cell lines (U251, U87, A172, T98G, LN229 and N3) detected by qRT-PCR. (B) Transfection efficacy of sh-LBX2-AS1#1, sh-LBX2-AS1#2 and sh-LBX2-AS1#3 in N3 and U87 cells detected by qRT-PCR. (C) Transfection efficacy of pcDNA-LBX2-AS1 in N3, U87 and U251 cells detected by qRT-PCR. (D) Relative levels of LBX2-AS1 in normal brain specimens, primary and recurrent GBM specimens. (E) Positive expressions of LBX2-AS1 in normal brain specimens, primary and recurrent GBM specimens measured by RNA-FISH. Scale bar=50μm. (F) Heatmaps of differentially expressed mRNAs in GBM samples from TCGA (upper lane) and CGGA (bottom lane) categorized into high group and low group based on the median level of LBX2-AS1. (G) Volcano plots showing the upregulated mRNAs regulated by LBX2-AS1 in GBM samples from TCGA (left side) and CGGA (right side). (H) GSEA analysis revealed the correlation between LBX2-AS1 and EMT, angiogenesis, and extracellular matrix disassembly in GBM samples. *p<0.05, **p<0.01, ***p<0.001.

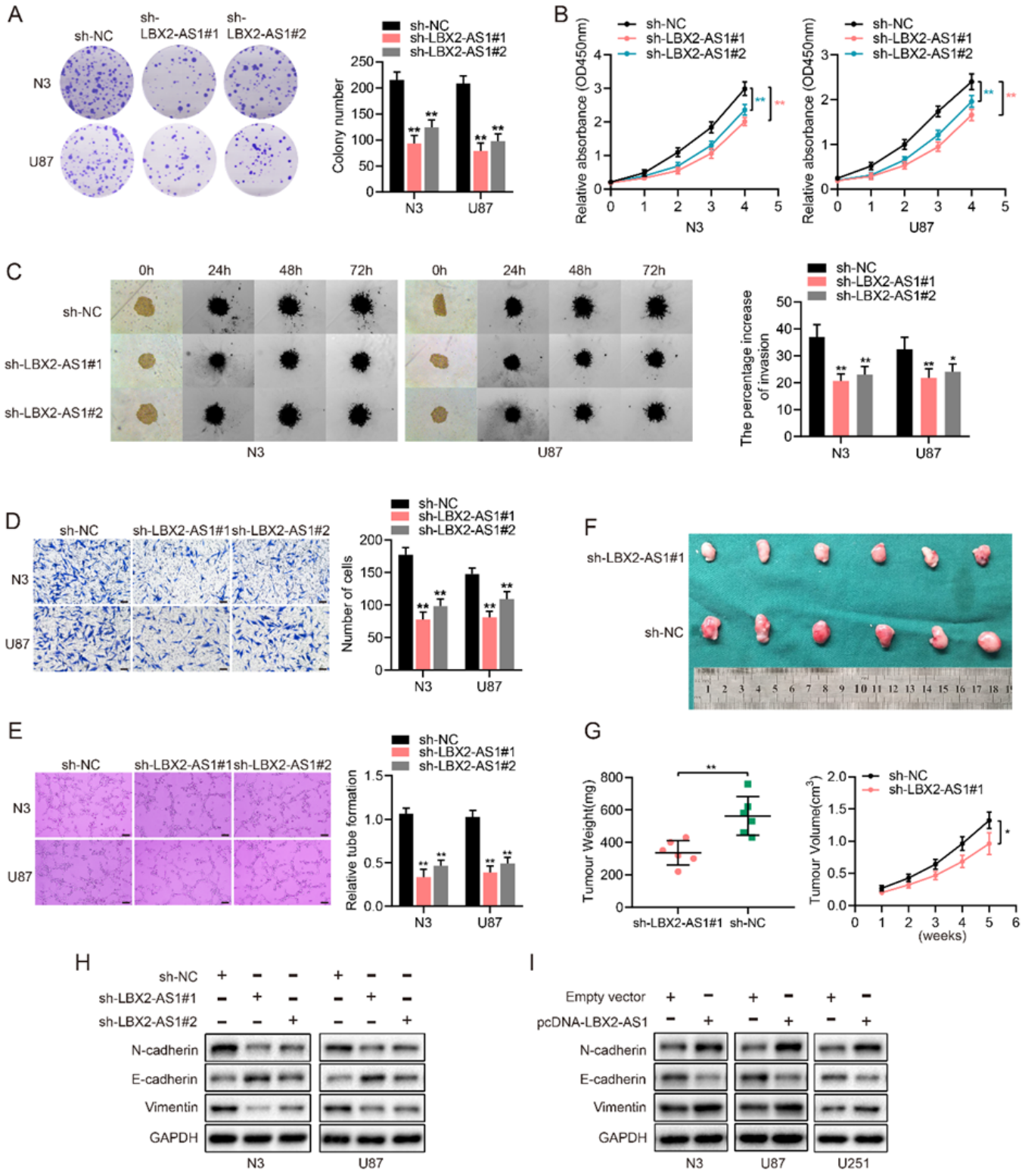

Figure 3

Knockdown of LBX2-AS1 suppresses cell proliferation, angiogenesis and EMT of GBM. (A, B) Proliferation of N3 and U87 cells with LBX2-AS1 knockdown examined by colony formation assay (A) and CCK-8 assay (B). (C, D) Invasion of N3 and U87 cells with LBX2-AS1 knockdown examined by 3D tumor spheroid invasion assay (C) and transwell assay (D). Scale bar = 100 μm. (E) Representative images (left side) and quantification (right side) of tube formation of HUVECs cultivated in conditioned

medium of N3 and U87 cells with LBX2-AS1 knockdown. Scale bar = 100 μm. (F) Representative image of subcutaneous tumors in nude mice administrated with U87-sh-LBX2-AS1#1 cells or U87-sh-NC cells. (G) Tumor weight (left side) and tumor volume (right side) of xenograft models. (H, I) Protein levels of EMT markers (N-cadherin, E-cadherin and Vimentin) in N3, U87 and U251 cells with knockdown (H) or overexpression (I) of LBX2-AS1. GAPDH was the internal reference. *p<0.05, **p<0.01.

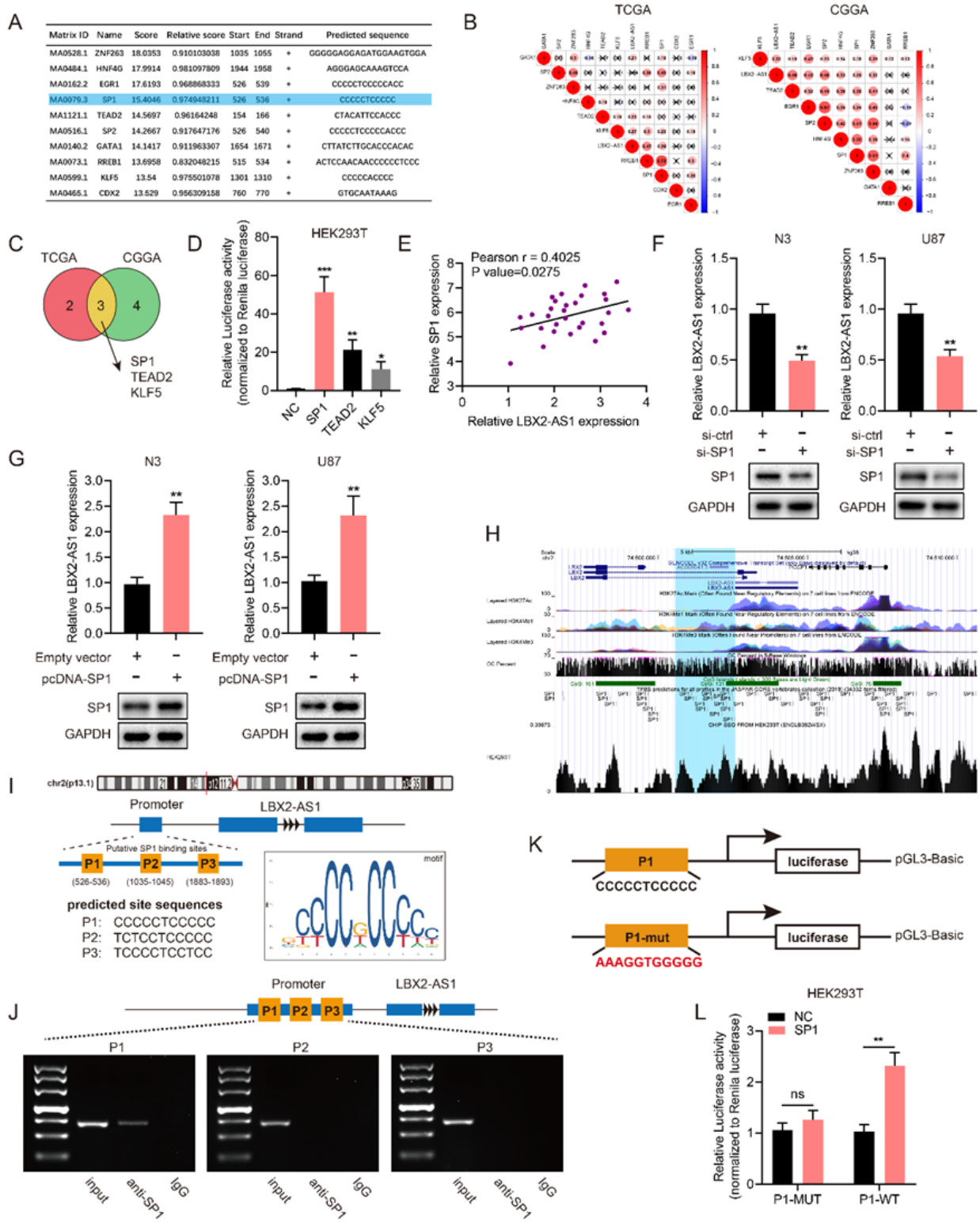

Figure 4

Sp1 upregulates LBX2-AS1 in GBM samples. (A) The top 10 scored transcription factors that could bind to the promoter region of LBX2-AS1 screened using JASPAR. (B) Spearman correlation analysis on the correlation between LBX2-AS1 and selected transcription factors in TCGA (left side) and CGGA databases (right side). (C) Venn diagram showing three transcription factors (Sp1, TEAD2, KLF5) that were intersected in both TCGA and CGGA by Spearman correlation analysis (Pearson r>0.2). (D) Luciferase activity of the binding between three transcription factors and LBX2-AS1. (E) Correlation between relative levels of LBX2-AS1 and Sp1 in 30 clinical specimens of GBM. (F, G) Relative level of LBX2-AS1 in N3 and U87 cells with knockdown (F) or overexpression (G) of Sp1. (H) Highly enriched Sp1 in the promoter region of LBX2-AS1 (highlighted in blue) in JASPAR and ENCODE databases. (I) Predicted sites where Sp1 bound to the promoter region of LBX2-AS1. (J) ChIP-PCR showing the enrichment of Sp1 in P1 site of the promoter region of LBX2-AS1; (K, L) Dual-luciferase reporter assay showing no significant influence of Sp1 on the luciferase activity of P1-mut. *p<0.05, **p<0.01, ***p<0.001.

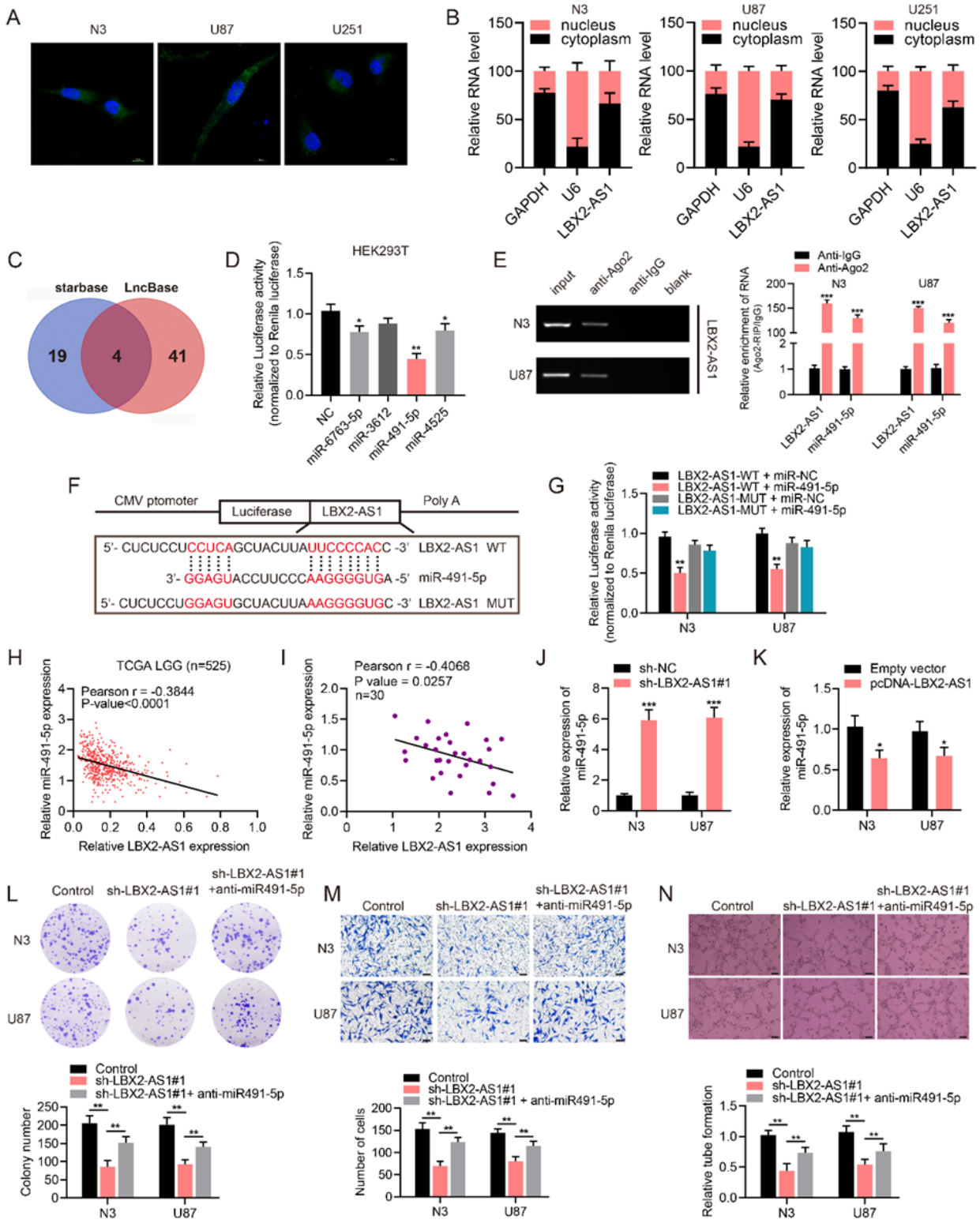

Figure 5

LBX2-AS1 exerts a sponge effect on miR-491-5p. (A) Subcellular distribution of LBX2-AS1 in N3, U87 and U251 cells. Scale bar = 10 μm. (B) Cytoplasmic and nuclear levels of LBX2-AS1 in N3, U87 and U251 cells detected by qRT-PCR. (C) Four candidate miRNAs with complementary sites to LBX2-AS1 predicted using starBase and LncBase. (D) Luciferase activity in the four miRNA vectors containing LBX2-AS1 promoter region in HEK293T cells. (E) Co-immunoprecipitants of LBX2-AS1 and miR-491-5p in anti-Ago2 and anti-

IgG. (F) Wild-type (WT) and mutant-type (MUT) luciferase vectors synthesized based on the predicted binding sites of miR-491-5p and LBX2-AS1. (G) Luciferase activity in N3 and U87 cells co-transfected with WT or MUT luciferase vectors with either miR-491-5p mimics or negative control. (H, I) Correlation between miR-491-5p and LBX2-AS1 in low-grade glioma samples from TCGA (H) and GBM samples from our center (I). (J, K) Relative level of miR-491-5p in N3 and U87 cells with knockdown (J) or overexpression (K) of LBX2-AS1. (I) Colony formation in N3 and U87 cells transfected with sh-LBX2-AS1#1 or miR-491-5p inhibitor + sh-LBX2-AS1#1. (M) Invasion in N3 and U87 cells transfected with sh-LBX2-AS1#1 or miR-491-5p inhibitor + sh-LBX2-AS1#1. (N) Representative images (upper lane) and quantification (bottom lane) of tube formation of HUVECs cultivated in conditioned medium of N3 and U87 cells transfected with sh-LBX2-AS1#1 or miR-491-5p inhibitor + sh-LBX2-AS1#1. Scale bar = 100 μm. *p<0.05, **p<0.01, ***p<0.001.

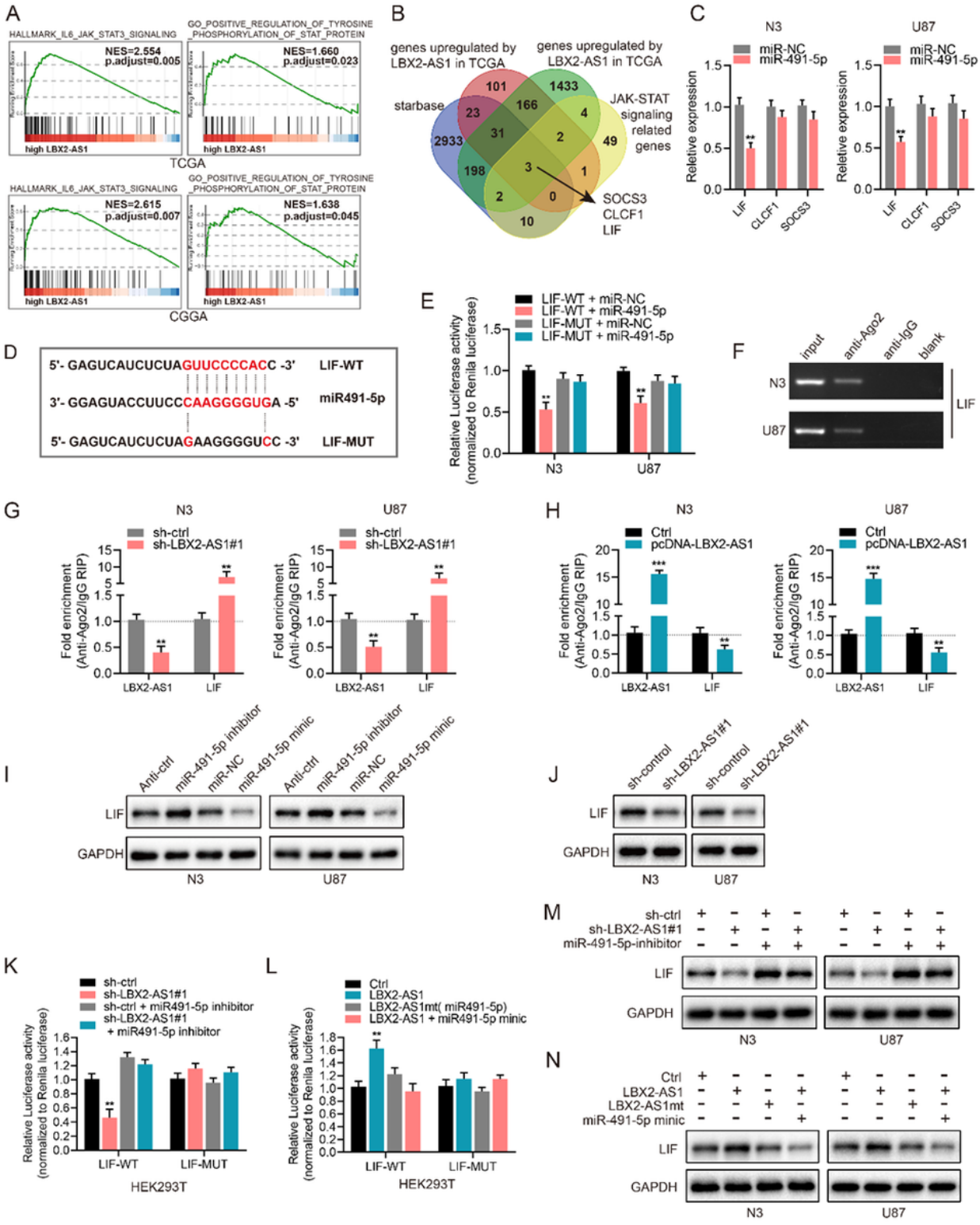

Figure 6

LIF is the target mRNA of miR-491-5p and indirectly regulated by LBX2-AS1. (A) Correlation between LBX2-AS1 and the JAK-STAT3 signaling pathway analyzed using GSEA. (B) Venn diagrams showing the candidate genes of miR-491-5p. (C) Relative levels of the three candidates in N3 and U87 cells transfected with miR-NC or miR-491-5p mimics. (D) Complementary sequences of LIF 3'-UTR to that of miR-491-5p, and the mutant sequences. (E) Luciferase activity of LIF-WT and LIF-MUT in N3 and U87

cells transfected with miR-NC or miR-491-5p mimics. (F) Enrichment of LIF in anti-Ago2 and anti-IgG. (G) Enrichments of LBX2-AS1 and LIF in anti-Ago2 in N3 and U87 cells with LBX2-AS1 knockdown. (H) Enrichments of LBX2-AS1 and LIF in anti-Ago2 in N3 and U87 cells overexpressing LBX2-AS1. (I) Protein level of LIF in N3 and U87 cells regulated by miR-491-5p. (J) Protein level of LIF in N3 and U87 cells with LBX2-AS1 knockdown. (K, L) Luciferase activity of LIF-WT and LIF-MUT in N3 and U87 cells co-regulated by LBX2-AS1 and miR-491-5p. (M, N) Protein level of LIF in N3 and U87 cells co-regulated by LBX2-AS1 and miR-491-5p. GAPDH was the internal reference. **p<0.01, ***p<0.001.

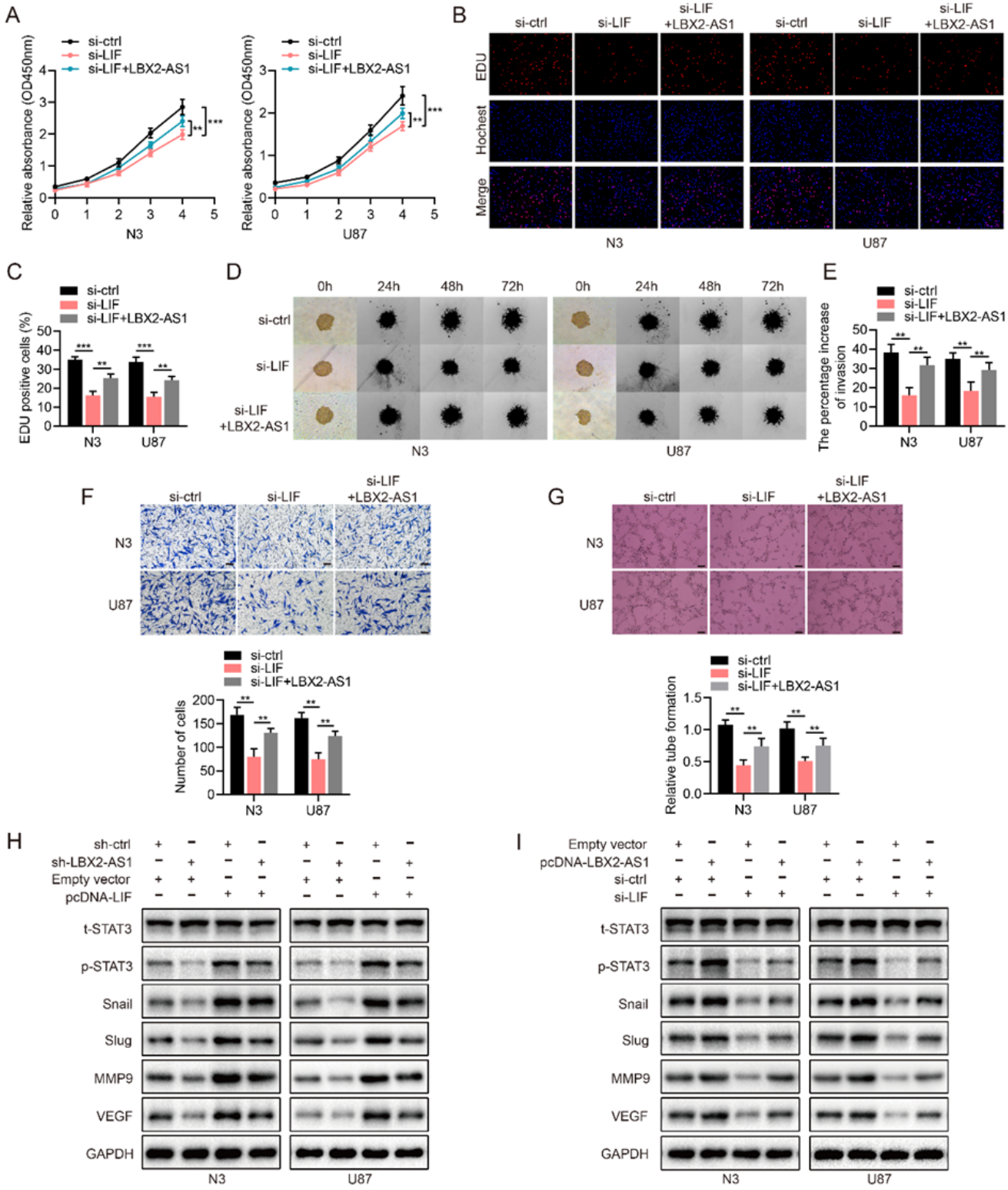

Figure 7

LIF advances malignant phenotypes of GBM cells via the LIF-STAT3 axis. (A-C) Proliferation of N3 and U87 cells regulated by LIF and LBX2-AS detected by CCK-8 assay (A) and EdU assay (B, C). (D-F) Invasion of N3 and U87 cells regulated by LIF and LBX2-AS examined by 3D tumor spheroid invasion assay (D, E) and transwell assay (F). Scale bar = 100 μm. (G) Representative images (upper lane) and quantification (bottom lane) of tube formation of HUVECs cultivated in conditioned medium of N3 and U87 cells regulated by LIF and LBX2-AS. Scale bar = 100 μm. (H, I) Protein levels of t-STAT3, p-STAT3, Snail, Slug, MMP9 and VEGF in N3 and U87 cells regulated by LIF and LBX2-AS. GAPDH was the internal reference. **p<0.01, ***p<0.001.

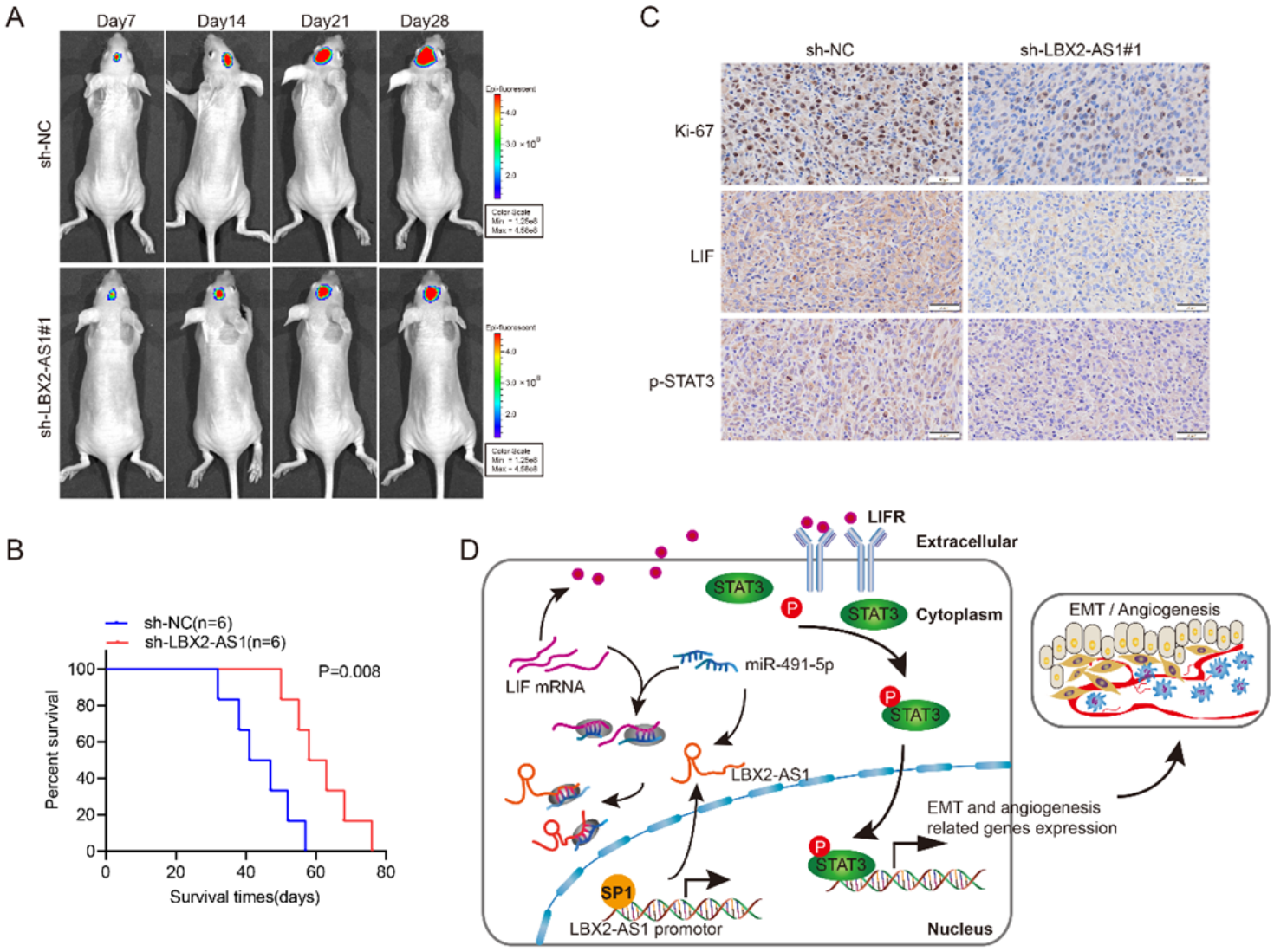

Figure 8

Knockdown of LBX2-AS1 slows down the growth of tumor in vivo. (A) Representative optical imaging of xenograft glioma in nude mice intracranially administrated with luciferase-labeled U87 cells transfected with sh-LBX2-AS1#1 or sh-NC. (B) Kaplan-Meier survival curves showed a better prognosis in LBX2-AS1 knocking-down group than the control group. (C) Immunohistochemical staining of Ki-67, p-STAT3 and

LIF in tumor sections. (D) Schematic diagram of the mechanism of LBX2-AS1 in promoting the malignant development of GBM.

Supplementary Files

This is a list of supplementary files associated with this preprint. Click to download.

- additionalfile1table.s13.docx
- additionalfile2table.s45.docx
- additionalfile3table.s67.docx
- additionalfile4figure.s1.docx
- additionalfile5figure.s2.docx
- additionalfile6figure.s3.docx
- additionalfile7figure.s4.docx